JOURNAL OF MATERIALS SCIENCE 26 (1991) 5309–5317

Superplasticity–dislocation creep interactions in a coarse grained Al–Cu–Zr alloy

K. A. PADMANABHAN
Department of Metallurgical Engineering, Indian Institute of Technology, Madras 600 036, India

J. HIRSCH
Fabrication Technology Division, Aluminium Company of America, Alcoa Center, Pittsburgh, PA, 15069 USA

K. LÜCKE
Institut für Allgemeine Metallkunde und Metallphysik, RWTH Aachen, Kopernikus Strasse 14, D 5100 Aachen, FRG

Specimens of a relatively coarse-grained Al–5.8Cu–0.39Zr (wt %) alloy were deformed at 730 K in tension by various amounts and at several strain rates. By comparing the grip and gauge (deformed) portions of each tested sample, taking into account the variations in the initial texture and using an orientation distribution function evaluation, the texture changes due to superplastic flow were identified. Crystallographic slip is shown to be significant only beyond the strain-rate range for maximum elongation. At lower strain rates, grain/interphase boundary sliding appears to control the deformation. The accompanying grain rotation causes a general weakening of the initial texture. It is also shown that evaluating an average value of the strain-rate sensitivity index, m, from a double logarithmic plot of the flow stress and true strain rate is inadequate for delineating the ranges of operation of different mechanisms. Instead, the evaluation of m by the changing strain rate method is advocated.

1. Introduction

The transmission electron microscopic (TEM) evidence that dislocation activity is minimal during superplastic flow has been questioned by Edington *et al.* [1]. Instead, they have advocated a study of the texture changes accompanying superplastic deformation for elucidating the mechanism(s) of flow. It has been pointed out that the texture changes reflect the entire thermo-mechanical history of the material and that the techniques of measurement involve much larger volume (than in the TEM methods) and a considerable degree of averaging. However, pole figures are regarded as qualitative and the determination of the (three-dimensional) orientation distribution functions (ODFs) is considered to be essential for drawing unequivocal conclusions.

Laudable though the aim was, as noted by Padmanabhan and Lücke [2], the resolution of the ODFs presented by Edington and co-workers [3–6] is inadequate by contemporary standards. The latter have also not considered the specimen to specimen variations in the starting texture. In fact, even in the same specimen, a through-thickness variation in texture may vitiate the results because, following large deformation, the grains in the interior reach the surface. Thus, there is a danger that in the absence of controlled experimentation and careful interpretation, this powerful technique may be used to make not so relevant statements about the operating mechanisms of flow.

Keeping the above in mind, the texture changes resulting from the superplastic deformation of one laboratory-prepared and two commercial aluminium alloys were measured and analysed using the ODF method. A brief report on the behaviour of the laboratory-made alloy of composition similar to Supral 100 (a commercial alloy) was presented recently [7]. The present paper is a detailed account of the findings and their implications. Descriptions of the response of the commercial alloys will appear elsewhere.

2. Experimental procedure

Ghosh and Raj [8–10] have suggested that during superplastic deformation (because of the presence of a grain-size distribution in the starting material), the fine grains deform by a diffusional process, while the coarse grains are subject to dislocation creep. The externally observed mechanical response is a weighted sum of these two physical processes. The commercial Supral 100 alloy has a grain size in the range 2–3 μm. Therefore, the present alloy was made in the laboratory with a coarser grain size of the order of 20 μm for two reasons: (a) to check if the mechanism of flow in the region of maximum ductility changes to predominantly dislocation creep (on account of the significantly larger grain size), and (b) to evaluate the extent of dislocation slip in a material of this kind, which can be taken as a safe upper limit of the contribution from this process to superplastic flow. (Needless to say, the

0022–2461/91 $03.00 + .12

coarser grain size will considerably decrease the absolute value of the elongation at fracture, but as the aim is to study only the nature of the operating mechanisms, this is of no serious consequence.)

The procedure of casting the alloy and reducing it to slabs 6 mm thick using forging and rolling is described elsewhere [11].

In thin specimens (thickness $\simeq$ 1–2 mm) grains from the interior appear at the surface after some deformation [12] and, if variations in texture are present in the thickness direction, interpretation can become difficult [13]. Therefore, from the 6 mm thick plates, tensile specimens of gauge dimensions 25 mm × 6.25 mm × 4 mm (ASTM sub-standard size) were machined keeping the axis of the specimens always parallel to the rolling direction. By sectioning, it was possible to study always the mid-thickness plane for the texture changes accompanying superplastic deformation and in this way any possible effects of a through-thickness variation in texture that could have been present, were eliminated.

The average initial grain size, as determined by the linear intercept method, was 20.2 ± 2.5 μm, which increased to 21.7 ± 3.4 μm on heating the specimen to the temperature of superplastic deformation. There was no observable grain elongation in the starting material.

Three specimens were chosen at random and subjected to chemical analysis. The alloy had the following composition (wt %): Cu 5.80, Zr 0.39, Fe 0.24, Zn 0.16, Si 0.13, Ni 0.062, Bi 0.036, Mg 0.01, Mn < 0.01, Ti 0.006, Al balance. The optimal temperature of superplastic deformation for Supral 100 is around 730 K [6]. Therefore, at 730 K, using a Zwick electromechanical testing machine, pre-determined superplastic strains, ranging from about 20% true strain to the elongation at fracture, were imparted at ten different (constant) rates of extension that varied from 0.40–99.00 mm min^{-1} (the initial strain-rate range was 2.7×10^{-4}– 6.6×10^{-2} s^{-1}). In order to achieve maximum accuracy, the temperature settings for the three coils in the furnace were fixed once and left undisturbed until the completion of all the experiments. By placing thermocouples at different points in the furnace, the pull rods and the elongating specimen, it was ensured that the control of temperature over the entire specimen length was always better than ± 1.5 °C.

Likewise, by measuring directly the elongation of specimen in a few cases covering the full load range of the tests and by obtaining this value also from the X–Y recorder output of the testing machine, a calibration chart was prepared. This enabled the determination of the true elongation of the specimen in the gauge portion by eliminating the contributions from grip flow and the elastic response of the testing system (pull rods, grips etc.). The tension tests revealed that at any given strain rate there was significant scatter in the linear flow stress–true strain plots. This has been traced to variations in the distribution of boundary pinning particles in the different specimens (unpublished work).

To ensure meaningful results, linear stress–strain curves of specimens elongated at a given crosshead speed by different amounts were superimposed, and only those specimens whose curves nearly coincided in the region of comparison were accepted for texture measurements. (Even this procedure did not guarantee that the starting textures were identical – see later.)

From the load–extension curves, a $\log\sigma_s$–$\log\dot{\varepsilon}_s$ plot was derived, where σ_s is the steady state flow stress and $\dot{\varepsilon}_s$ is the corresponding true strain rate. (In conformity with earlier practice [12], in all tests these two quantities were evaluated at a constant strain.) To identify correctly the different regions of superplastic flow (I, IIa, IIb and III, see Fig. 3.2b of [12]), the strain-rate sensitivity index, m, was measured directly by the change in strain-rate method (see Equation 2.31 of [12]), apart from obtaining it as the slope of the $\log\sigma_s$–$\log\dot{\varepsilon}_s$ plot. (For improved accuracy in the measured value of m, the difference between the two strain rates used in the tests should be small, which was the case in these experiments. As an additional correlation, the elongation to fracture was also determined as a function of strain rate.)

Texture measurements using X-rays were made on a fully automatic texture goniometer [14]. For each sample, four incomplete pole figures, (1 1 1), (2 0 0), (2 2 0), (1 1 3), were obtained in the reflection mode ($\alpha_{max} = 85°$). From these, three-dimensional ODFs were calculated using Bunge's method of series expansion with spherical harmonic functions [15, 16] and these were then ghost corrected by Gauss model calculations [17]. The results were obtained in the form of pole figures and the ODFs were plotted in sections of constant ϕ_2 in the Euler angle space defined by angles ϕ_1, ϕ_2 and ϕ. In order to eliminate the possible influence of a difference in the initial texture (which could not be ruled out), for each sample both the deformed portion, D, and the undeformed grip portion, G (which was exposed only to the elevated temperature), were examined. This way, the effects due to heating could be separated from those due to deformation.

3. Results

As indicated in the previous section, there was significant scatter in the mechanical properties due to chance variations in the starting microstructure/distribution of boundary pinning particles from one specimen to the next. In Fig. 1 $\log\sigma_s$–$\log\dot{\varepsilon}_s$ plot is presented, which has been derived from those tension tests accepted for subsequent texture analysis following the procedure outlined in Section 2. It is seen that for a major part of the plot $m = 0.34$. However, when m was evaluated directly by the method of changing strain rate [12], it went through a maximum with strain rate, as did the elongation to fracture (see Fig. 9 and the following sections for details).

The initial texture had the character of f c c rolling textures (Fig. 2a and b). The orientation distribution formed a tube (β fibre) through the orientation space. A comprehensive description and comparison of different samples is possible by plotting the orientation density maxima $f(g)$ along the β fibre and their exact position in the orientation space, defined by ϕ_1, ϕ and

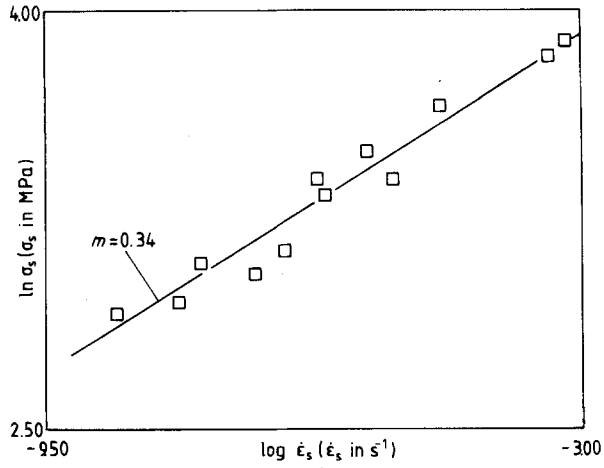

Figure 1 The log–log plot of the steady state true stress, σ_s–true strain rate, $\dot{\varepsilon}_s$, relationship (determined at a constant strain) for the laboratory-made alloy.

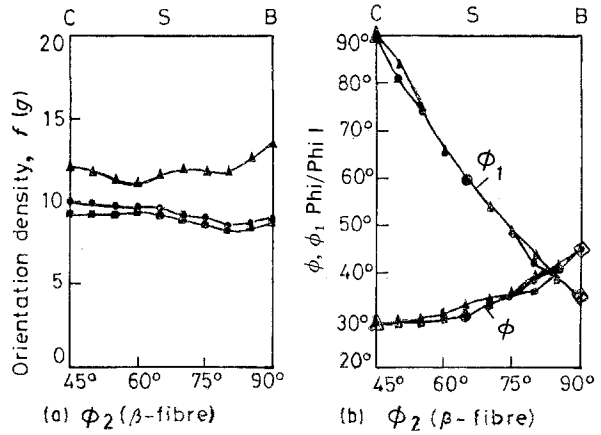

Figure 3 (a) Orientation density maxima along the β fibre, and (b) their positions in the orientation space.

ϕ_2 [18–20]. The main orientations on this tube are C ≃ {1 1 2}⟨1 1 1⟩ (90°, 35°, 45°); S ≃ {1 2 3}⟨6 3 4⟩ (59°, 36°, 63°) and B ≃ {0 1 1}⟨2 1 1⟩ (45°, 45°, 90°) (Fig. 3a and b).

Fig. 4a shows a typical example of the texture change after an elongation of 140% at an extension rate of 2.5 mm min^{-1} ($\dot{\varepsilon}_s = 6.9 \times 10^{-4}$ s^{-1}). Rolling-type texture still persists, but the intensity is weaker than in the starting material (cf. Fig. 2a). A similar result is also seen in the grip region (Fig. 4b). However, this texture shows additionally in the low-intensity regions some diffuse spreading of new orientations. This effect was common to all the samples and indicates a certain amount of primary recrystallization.

These effects are clearer in the ODFs, e.g. in a sample deformed by 120% at an extension rate of 4 mm min^{-1} ($\dot{\varepsilon}_s = 1.2 \times 10^{-3}$ s^{-1}) (Fig. 5a and b). In the grip region, cube and rolling direction (RD)-rotated cube orientations had increased.

The high resolution of the ODFs also revealed some differences in the details of the main texture peaks. In the grip region the texture was generally flattened, but

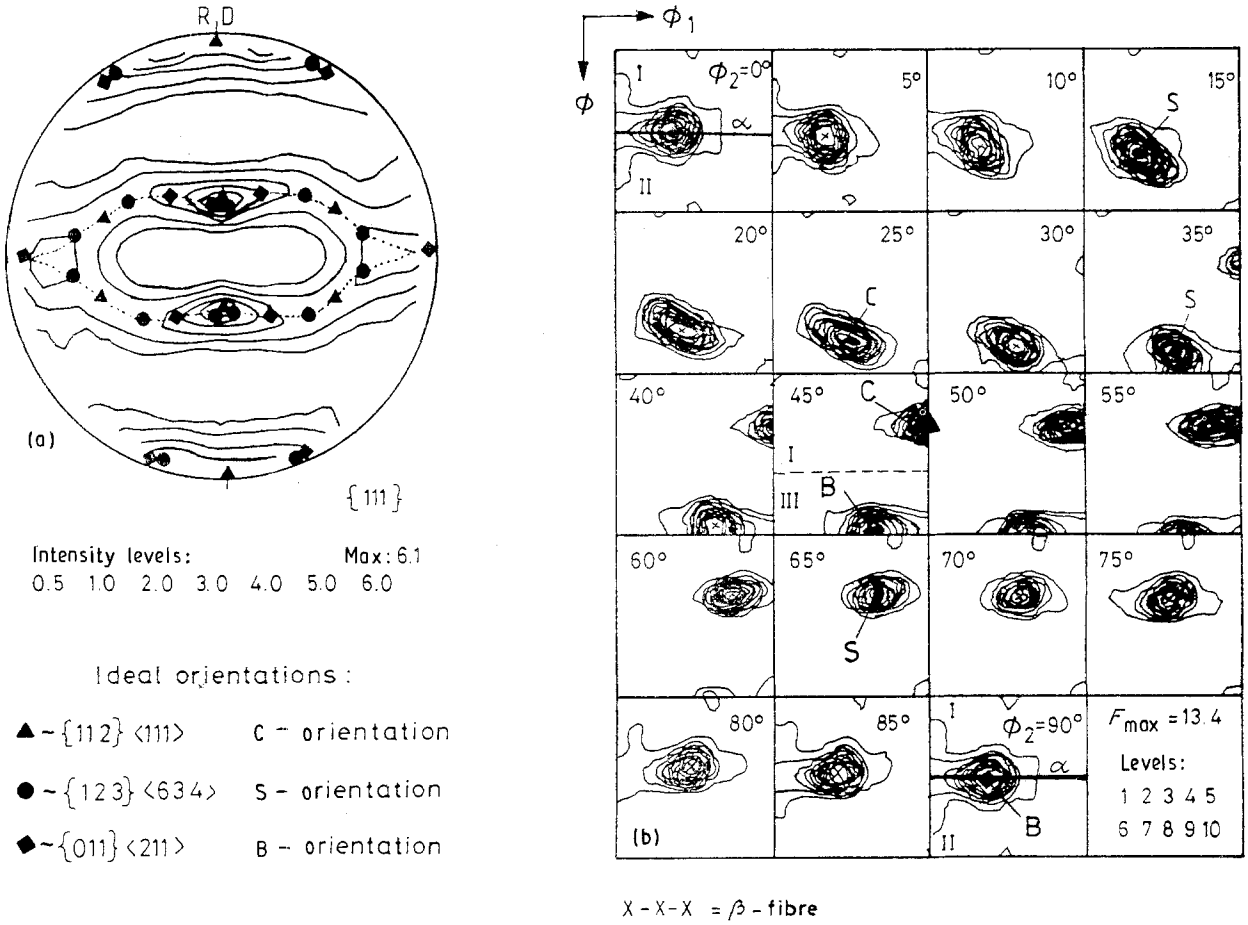

Figure 2 (a, b) Fcc rolling texture seen in the laboratory-made alloy (starting condition).

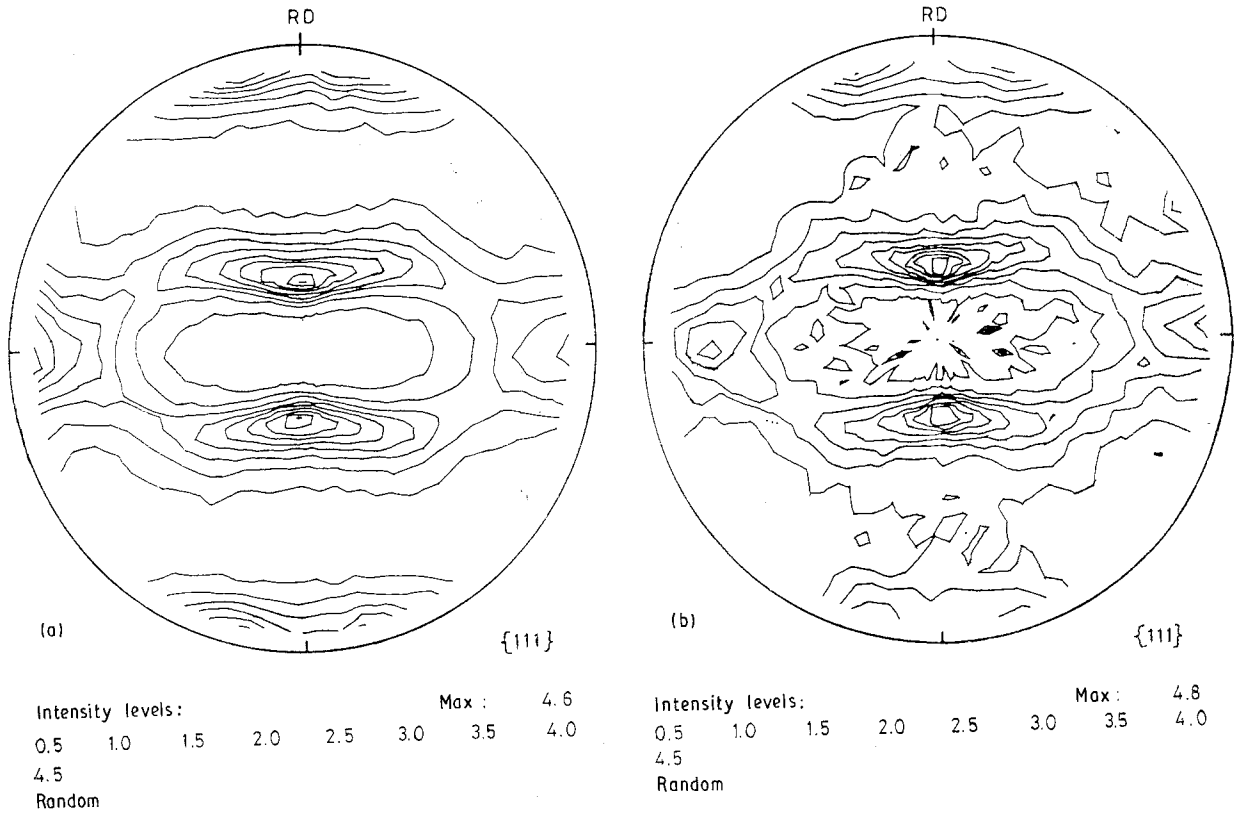

Figure 4 Pole figures showing typical texture changes in a specimen tested at an extension rate of 2.5 mm min^{-1} ($\dot{\varepsilon}_s = 6.9 \times 10^{-4}$ s^{-1}): (a) deformed region; (b) grip region.

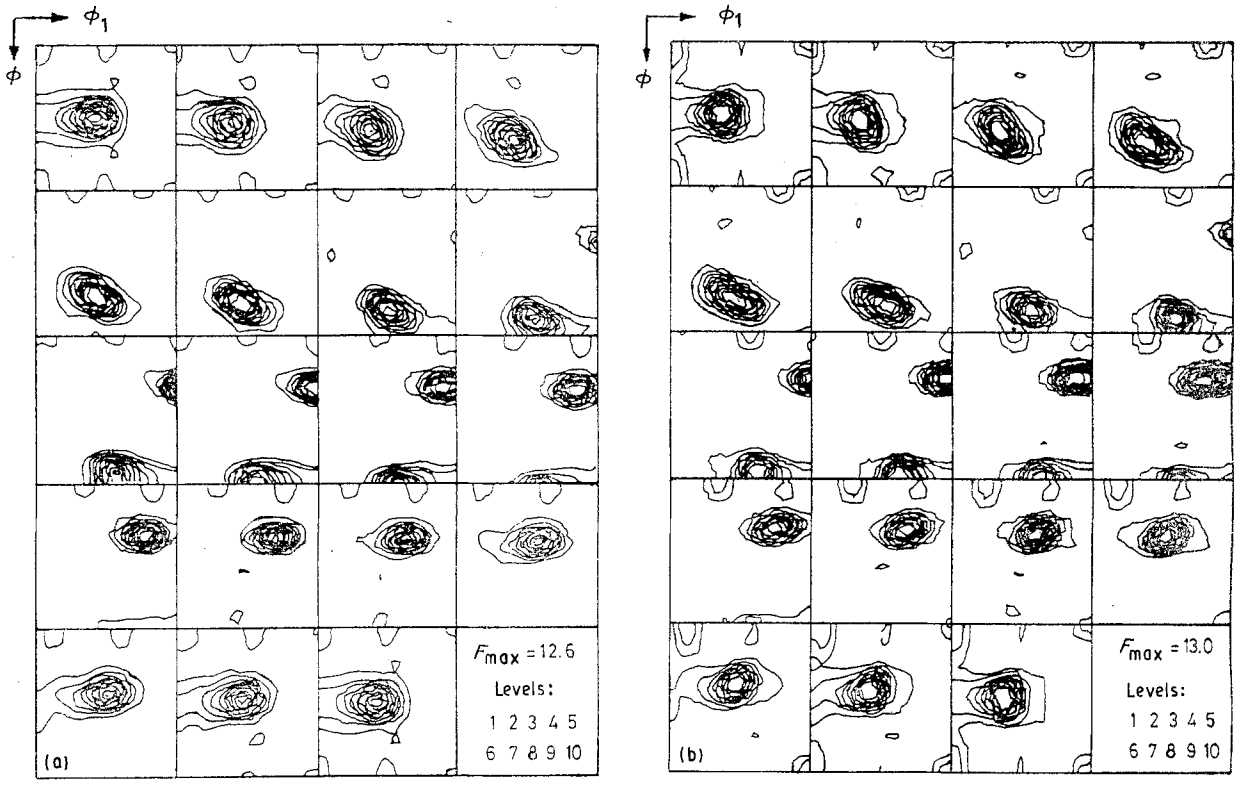

Figure 5 ODFs in a specimen elongated by 120% at 4 mm min^{-1} ($\dot{\varepsilon}_s = 1.2 \times 10^{-3}$ s^{-1}): (a) deformed region; (b) grip portion.

in the deformed (gauge) portion it showed a systematic scattering spreading (Fig. 5a). This was most pronounced in the B orientation ($\phi_2 = 0°$ or 90°) which was widely scattered in the direction of ϕ_1, i.e. around the normal direction (ND) At higher strain rates even a significant shift of the peak maximum itself was seen.

The changes in the rolling texture orientations are observed best in the skeleton line plots. In Figs 6 and 7 the maximum density along the β fibre (Figs 6a and 7a) and their exact position in the Euler space (Figs 6b

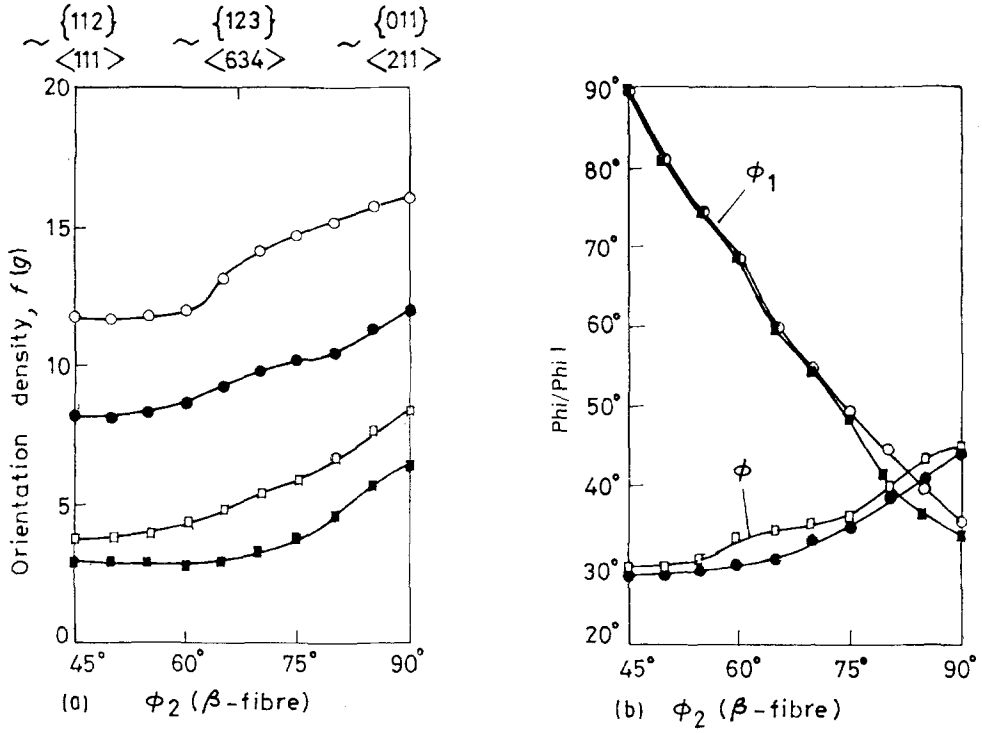

Figure 6 (a) Orientation density maxima along the β fibre, and (b) their exact positions in the Euler space. Extension rate = 0.4 mm min^{-1} ($\dot{\varepsilon}_s = 2.7 \times 10^{-4}$ s^{-1}). (●, ■) G = grip portion, (○, □) D = deformed region. (●, ○) 20%, (■, □) 89%.

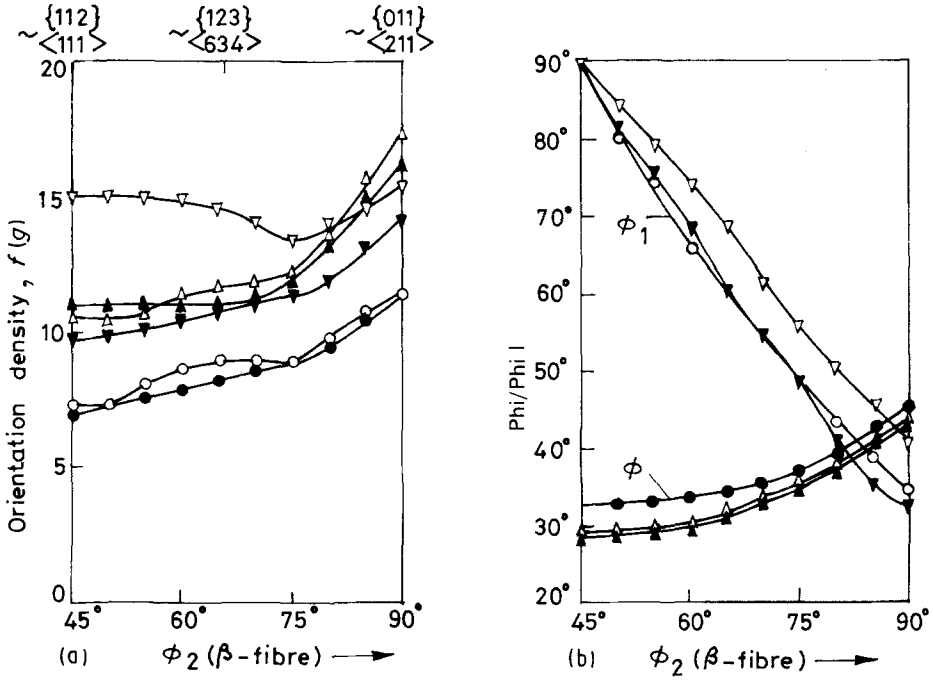

Figure 7 (a) Orientation density maxima along the β fibre, and (b) their exact positions in the Euler space for extension rates, $\dot{e}$, in the range 4–12 mm min^{-1}. (●, ▲, ▼) G, (○, △, ▽) D. (○, ●) 181%, $\dot{e} = 4$ mm min^{-1}; (△, ▲) 188%, $\dot{e} = 6$ mm min^{-1}; (▽, ▼) 183%, $\dot{e} = 12$ mm min^{-1}.

and 7b) are plotted for several samples deformed under different conditions. The following strain-rate dependent effects were identified.

(i) At a low extension rate of 0.4 mm min^{-1} ($\dot{\varepsilon}_s = 2.7 \times 10^{-4} s^{-1}$) (Fig. 6), a systematic decrease in the orientation density with strain was present. The texture of the deformed portion, D, was systematically sharper than that of the grip region, G (Fig. 6a). Little change in the β fibre position had occurred (Fig. 6b).

(ii) At a near-constant strain of 180% and extension rates in excess of what is depicted in Fig. 6, the decrease in the orientation density was much less and at extension rates greater than 9.0 mm min^{-1} ($\dot{\varepsilon}_s \gtrsim 6.0 \times 10^{-3}$ s^{-1}) it even appeared to increase near the C orientation ($\phi_2 = 45°$, cf. Figs 3a and 7a). In these samples systematic shifts in the β position could also be observed (Fig. 7b) which for the B orientation ($\phi_2 = 90°$) tended to higher ϕ_1 (approximately ND

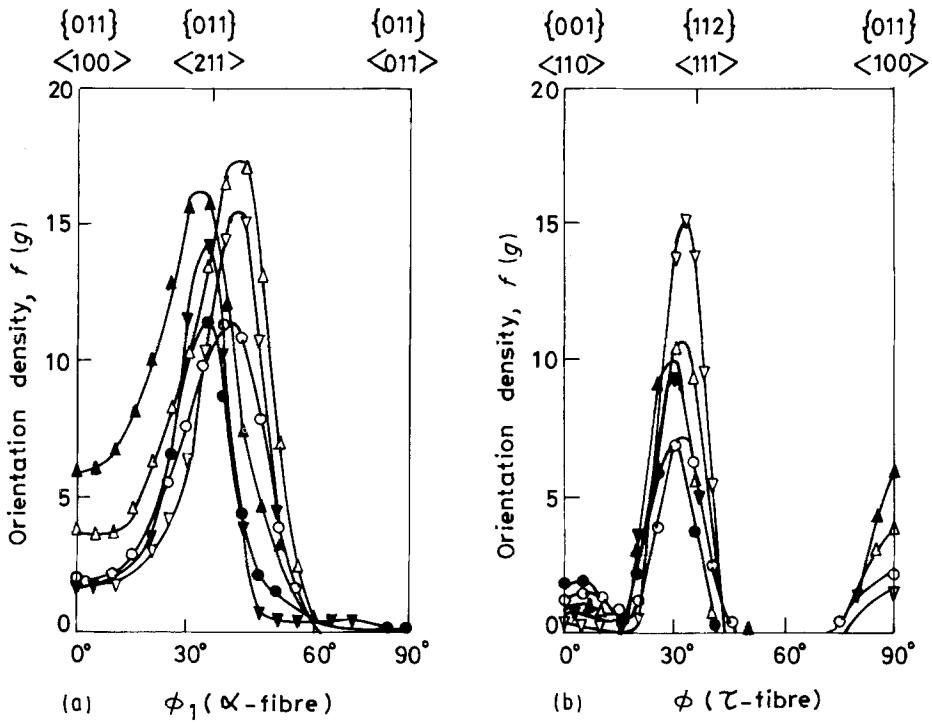

Figure 8 Shift of the β fibre position of (a) the B orientation, and (b) the C orientation, corresponding to the extension rates mentioned in Fig. 7. (●, ▲, ▼)G, (○, △, ▽) D.

rotation), and for the C orientation ($\phi_2 = 45°$) to higher ϕ (approximately transverse direction (TD) rotation). These shifts could be observed better in the intensity plots around these orientations along the corresponding angles (along ϕ_1 for B and ϕ for C, Fig. 8a and b). Clearly the ϕ_1 shift of the B orientation is stronger than that for the C orientation along ϕ.

4. Discussion

We appreciate the fact that using one of the early programs due to Kallend [21], Edington and coworkers [1, 3–6] tried to apply a newly emerging, powerful analytical technique (the ODF analysis) to a problem of both fundamental and technological significance. Unfortunately, the angular spacing used by them was 10°, whereas by present standards a spacing of 5° is required. Moreover, at that point in time, the possible existence of "ghosts" in the ODFs was unknown and so the authors could not obtain the true ODFs. Edington *et al.* also did not undertake a systematic study to separate the thermal effects from those due to superplastic deformation. Thus it must be noted that their conclusions are based on insufficient evidence/analysis.

In this investigation, on the other hand, by comparing the (superplastically) deformed, D, and grip, G, regions of the same sample the texture changes due to superplastic flow could be separated. In the grip portion the formation of new texture components in random orientations or in the form of the cube and RD-rotated cube orientations (Fig. 5b), indicates conventional primary recrystallization. This process appears to be suppressed in the gauge (deformed) portion. It could be argued that in the gauge portion also some form of recrystallization, which is not permitted to develop new peaks because of the accompanying deformation, was present. But a systematic spread of the B orientation ($\phi_2 = 90°$) in the direction of ϕ_1 around ND is present in Fig. 5a. This is clear evidence for grain rotation.

It would appear, therefore, that in the grip region primary recrystallization causes a general weakening of the initial texture. In the gauge portion grain rotations (which can only result from grain/interphase boundary sliding controlled flow, as crystallographic slip was negligible at low strain rates – see later) reduce the texture intensity. This latter process is slower than primary recrystallization in weakening the initial texture (e.g. compare the texture intensities of the grip and gauge portions in Fig. 6a). Thus it has been possible for the first time to distinguish between texture weakening due to primary recrystallization (a thermal effect) and the flattening of texture peaks because of grain rotations accompanying superplastic flow. (In view of the above, the evidence for "dynamic recrystallization" in the Supral alloys reported based on transmission electron microscopy (see, for a summary, [22]) should be examined more closely).

Bowen and Hirsch [23] have also published some ODF results and compared them to the microstructure present in several superplastically deformed aluminium alloys. Their conclusions support and supplement the above arguments. According to these authors small and equiaxed grains mostly deform by grain/interphase boundary sliding. When grain rotation is involved it leads to a decrease in the texture intensity. A pancake-shaped grain structure causes mainly in-plane grain rotation. But when elongated grains slide, they often preserve their orientations and there will be no large texture change. So grain shape has a strong influence on superplastic deformation. In some cases when the initial microstructure is elongated, the grains are not initially free to slide or rotate.

Then crystallographic slip also contributes to superplastic deformation causing systematic peak shifts, similar to those observed in the present investigation.

Nix [24] has argued that if at low strain rates boundary sliding–diffusion coupled flow is present and the latter controls the rate of deformation, as suggested by the Ashby–Verrall model [25], there is no way that the observed grain rotations can be explained. This is because deformation in that model cannot give rise to an internal torque, essential for grain rotations. On the other hand, in the model of Padmanabhan [26, 27] and the phenomenological treatment of Beere [28], the normal boundary stresses are assumed to relax quickly, which leaves the boundary shear stresses to support the aggregate. The shear stresses then control the deformation rate, i.e. grain/interphase boundary sliding is the rate-controlling mechanism. (As noted by Beere [28], hexagonal arrays have strength when either the boundary shear stress or the normal stress is relaxed to zero.) When the aggregate is deformed, energy is dissipated by sliding on the boundary. The energy expenditure is minimized if the grains are allowed to rotate [28]. Thus, grain rotation invariably accompanies boundary sliding. (In superplastic alloys the differences in the orientation and mobility of the different types of boundaries will give rise to the unbalanced boundary shear stresses essential for grain rotation.) Unlike in the case of crystallographic slip, these grain rotations can be in any direction and need not lead to systematic shifts in the orientation maxima towards stable end positions. Then a systematic overall weakening in the texture intensity with strain will result, which is observed in the present experiments as well as those of Bowen and Hirsch [23]. It is also interesting to note (a) that Nix [24] has conceded that the presence of an internal torque can give rise to grain rotations (even in the absence of crystallographic slip), and (b) that Wilkinson [29] has found the idea of grain/interphase boundary sliding control of flow useful for understanding grain growth in superplastic alloys.

It must be noted at this stage that barring the proposals of Padmanabhan [12, 26, 27] and Beere [28], all the others consider grain/interphase boundary sliding as an inherently fast process so much so that notwithstanding its preponderance, at no stage it is considered to be the rate-controlling process. (This is an assumption that is also common in most theories of high-temperature creep.) Often this is stated as self-evident; but Hazzledine [30] has offered an explanation. In the upper power law creep range sliding is much slower than the other independent deformation process of dislocation slip which determines the flow characteristics. In the lower power law creep region, even though it is faster than crystallographic slip, boundary sliding does not markedly change the stress–strain rate curve and the deformation remains limited by the grain strain rate whenever the grains are capable of homogeneous deformation. At still lower stresses, where the linked mechanisms of diffusive creep–grain boundary sliding operate, sliding is potentially faster than diffusive creep and does not control the rate of flow.

Evidently, the validity of the above statements critically depends on the accuracy of the various equations assumed to describe the different flow processes (along with all the inherent assumptions involved in their derivation) and not on any physically valid arguments. Thus, in our view, the simplest and logical way of understanding texture weakening at low strain rates seen in the present experiments (and many other earlier studies) is in terms of grain rotations accompanying grain/interphase sliding controlled flow.

In contrast, at high strain rates, some texture sharpening is seen in the deformed region, D, (Fig. 7a). Taken together with the observed scattering and shift of the β fibre (Figs 7 and 8) this reveals the increased importance of dislocation slip. As the direction of shift agrees with the Taylor theory, multiple slip is implied, wherein the B- and C-oriented grains are rotated into a position with ⟨1 1 1⟩ parallel to the tensile direction [31]. This is already reached in Fig. 8b for the C-oriented grains by a rotation to $\phi = 35°$, i.e. $\{1\,1\,2\}\langle 1\,1\,1\rangle$. A certain further accumulation of grains at this orientation causes the corresponding increase in intensity (Fig. 7a). For the B-oriented grains, however, a ϕ_1 rotation of 20° is necessary (towards $\{0\,1\,1\}\langle 1\,1\,1\rangle$ at $\phi_1 = 55°$) which is not yet reached at the imposed strain (Fig. 8a).

According to the Taylor theory, when the sole mechanism of flow is dislocation slip, a rotation rate of 1°/2.25% strain will be present. (Calculations based on this theory should provide an upper estimate of the independent contribution from crystallographic slip to superplastic flow because during superplastic deformation grain/interphase boundary sliding and diffusion also will aid dislocation slip in generating a given strain tensor.) Thus, knowing the changes in orientation at maximum strain, ϕ_i, the contribution from dislocation slip can be calculated. The results obtained in this fashion are presented in Fig. 9 as a function of strain rate, along with the elongation to fracture and the directly measured values of m. The average value of m, obtained from Fig. 1, is also shown within parentheses. (Crystallographic slip as a non-rate-controlling process could have been present to accommodate grain/interphase boundary sliding–diffusive flow. As the latter mechanism will then determine the nature of flow, and slip merely provides the necessary rapid accommodation, such a (slip) process due to its random nature will not influence the texture results [1].)

It is clear from the foregoing that even when the average grain size was greater than 20 μm, up to the strain rate corresponding to the maximum value of elongation at fracture, the contribution of slip (as an independent rate-controlling process) to total deformation was less than 10%. The strain-rate dependence in this region of the slip contribution was also weak. Beyond this strain-rate range the slip contribution rapidly increased with strain rate and reached a value of about 20% at the highest strain rates employed in these experiments. The presently observed trends agree well with the earlier (qualitative) results of Matsuki *et al.* [32], which were based on pole figure

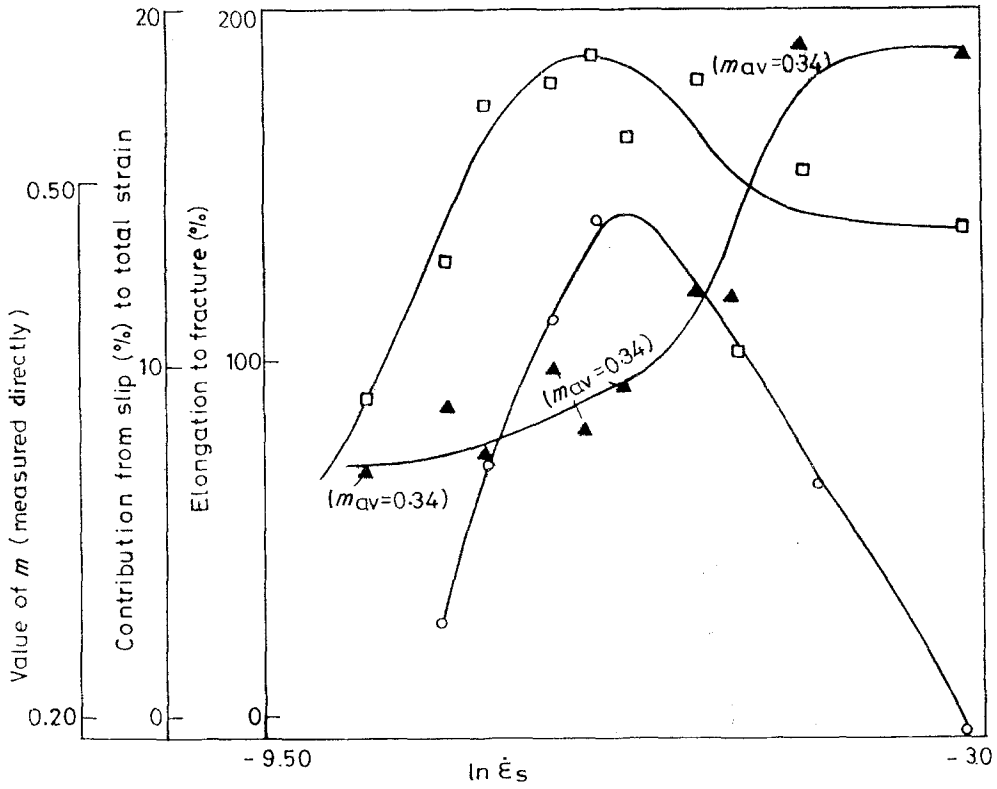

Figure 9 (□) The maximum elongation, (○) directly measured value of m and (▲) percentage contribution from slip to the total strain as functions of the true steady state strain rate. The average value of m is also given in parentheses at appropriate places.

measurements on an aluminium alloy of a smaller average grain size.

It is pertinent to note here that at the lower strain rates, even when the average grain size was in excess of 20 μm the importance of slip did not increase significantly compared to what is reported for ultra-fine grained materials [1, 2, 6, 12]. This calls into question the suggestion [8–10] that the mechanical response seen during structural superplasticity is the result of the simultaneous deformation of the fine grains by a diffusive process and the coarse grains by dislocation creep. Further the model [8–10] involves a number of ill-defined parameters [33], does not take into account explicitly (or predict) the presence of important (superplasticity) events like grain boundary sliding, grain rotation, grain switching and the emergence of new grains at the surface, and also makes the unlikely assumption of the existence of uniform strain in all the grains, regardless of the grain size and the operating mechanism. (This last assumption is common in high-temperature creep, where the grain size dependence of the creep rate is negligible. In superplasticity, on the other hand, the grain size dependence of strain rate is strong and significant grain/interphase boundary sliding is available as an additional mechanism to achieve strain compatibility.)

The present study also reveals that considering only an average value of m (obtained as the average slope of a $\log\sigma_s$–$\log\dot{\varepsilon}_s$ plot), although acceptable for superplastic forming, is inadequate for understanding the mechanisms of superplasticity. In the present case, practically over the entire range of strain rates employed an average value of m equal to 0.34 could be obtained (Figs 1 and 9). However, the elongation to fracture decreased and the contribution of crystallographic slip to the total deformation increased above a certain strain rate and this could not be understood in terms of an average m value assigned for the entire range. This may explain why various authors have drawn different conclusions on the importance of crystallographic slip to superplastic flow, even though ostensibly they all have evaluated the texture changes under peak m conditions (for a summary of these results, see [2]).

On the other hand, the direct method of evaluating m, which regards m as constant only over a very narrow strain-rate range (and hence is considered to be the best method of evaluating m [12]) correlates well with the elongation at fracture. It also reflects rather effectively the changes in the contribution of dislocation slip to the total strain (Fig. 9).

5. Conclusions

Based on a study of the texture changes accompanying superplastic deformation in an Al–5.8Cu–0.39Zr (wt %) alloy of average grain size 21.7 ± 3.4 μm, the following conclusions could be drawn.

1. Heating the alloy to the temperature of superplastic deformation gave rise to texture weakening by primary recrystallization (a thermal effect). Superplastic deformation tended to suppress this mechanism and promoted texture flattening by grain rotation. Owing to a difference in the rates of these processes it has been possible to distinguish, for the first time, between texture weakening due to recrystallization and that due to grain rotation.

2. The grain rotation seen at low strain rates that

caused a reduction in the texture intensity is a concomitant of grain/interphase boundary sliding controlled flow.

3. At strain rates up to that for which the elongation at fracture is maximum, the contribution of crystallographic slip to the total deformation was rather small. The strain rate dependence of this contribution in this range was also weak.

4. At strain rates greater than that for which the elongation to fracture is maximum, Taylor slip made a rapidly increasing contribution to the total deformation, which rose to about 20% at the highest strain rates employed in the present experiments.

5. The mechanisms of flow in the different ranges of strain rate did not change drastically in this coarse-grained alloy compared to what has been reported for ultra-fine grained materials. This observation is of relevance while considering the different theories of structural superplasticity.

6. The average value of m obtained as the average slope of a log flow stress–log true strain rate plot did not correlate well with the elongation to fracture and the changes in the operating mechanisms when these were evaluated as functions of strain rate. On the other hand, the m value obtained from the changing strain rate method [12] related well to these changes.

Acknowledgement

KAP thanks the Alexander von Humboldt-Stiftung for the award of an international fellowship.

References

1. J. W. EDINGTON, K. N. MELTON and C. P. CUTLER, *Prog. Mater. Sci.* **21** (1976) 61.
2. K. A. PADMANABHAN and K. LÜCKE, *Z. Metallkde* **77** (1986) 765.
3. K. N. MELTON and J. W. EDINGTON, *Scripta Metall.* **8** (1974) 1141.
4. K. N. MELTON, J. W. EDINGTON, J. S. KALLEND and C. P. CUTLER, *Acta Metall.* **22** (1974) 165.
5. C. P. CUTLER, J. W. EDINGTON, J. S. KALLEND and K. N. MELTON, *ibid.* **22** (1974) 665.
6. R. H. BRICKNELL and J. W. EDINGTON, *ibid.* **27** (1979) 1303.
7. J. HIRSCH, K. A. PADMANABHAN and K. LÜCKE, in "Proceedings of the 8th International Conference on Texture of Materials" (ICOTOM-8), edited by J. S. Kallend and G. Gottstein (Metals Society AIME, Warrendale, PA, 1988) p. 555.
8. A. K. GHOSH and R. RAJ, *Acta Metall.* **29** (1981) 283.
9. *Idem., ibid.* **29** (1981) 607.
10. *Idem.*, in "Proceedings of the International Conference on Superplasticity", edited by B. Baudelet and M. Suery (Centre Nationale de la Recherche, Paris, 1985) pp. 11.1–11.19.
11. K. A. PADMANABHAN, J. HIRSCH and K. LÜCKE, *J. Mater. Sci.* **26** (1991) 5301.
12. K. A. PADMANABHAN and G. J. DAVIES, "Superplasticity" (Springer-Verlag, Berlin/Heidelberg/New York, 1980) pp. 8–132.
13. K. HENNIG, A. MÜCKLICH, I. I. NOVIKOV, V. J. PORTNOY, V. M. ILENKO and S. MATTHIES, in "Proceedings of the 7th International Conference on Texture of Materials" (ICOTOM-7), edited by C. M. Brakman, P. Jongenburger and E. T. Mittemeijer (Netherlands Society for Materials Science, Noordwijkerhout, Netherlands, 1984) p. 499.
14. J. HIRSCH, G. BURMEISTER, L. HOENEN and K. LÜCKE, in "Experimental Techniques of Texture Analysis", edited by H. J. Bunge (DGM, Obernursel, FRG, 1986) p. 63.
15. H. J. BUNGE, "Mathematische Methoden der Texturanalyse" (Akademie, Berlin, 1969).
16. J. JURA and J. POSPIECH, *Texture* **3** (1978) 1.
17. K. LÜCKE, J. POSPIECH, K. H. VIRNICH and J. JURA, *Acta Metall.* **29** (1981) 169.
18. J. HIRSCH, PhD thesis, RWTH Aachen, FRG (1984).
19. J. HIRSCH and K. LÜCKE, *Acta Metall.* **36** (1988) 2863.
20. *Idem., ibid.* **36** (1988) 2883.
21. J. S. KALLEND, PhD thesis, University of Cambridge, UK (1970).
22. D. J. LLOYD and D. M. MOORE, in "Superplastic Forming of Structural Alloys", edited by N. E. Paton and C. H. Hamilton (Metals Society AIME, Warrendale, PA, 1982) p. 147.
23. A. W. BOWEN and J. HIRSCH, in "Proceedings of the 8th International Conference on Texture of Materials" (ICOTOM-8), edited by J. S. Kallend and G. Gottstein (Metals Society AIME, Warrendale, PA, 1988) p. 549.
24. W. D. NIX, in "Proceedings of the Symposium on Superplastic Forming", edited by S. P. Agrawal (American Society for Metals, Metals Park, OH, 1985) p. 3.
25. M. F. ASHBY and R. A. VERRALL, *Acta Metall.* **21** (1973) 149.
26. K. A. PADMANABHAN, *Mater. Sci. Engng* **29** (1977) 1.
27. *Idem., ibid.* **40** (1979) 285.
28. W. BEERE, *J. Mater. Sci.* **12** (1977) 2093.
29. D. S. WILKINSON, in "Proceedings of the International Conference on Superplasticity", edited by B. Baudelet and M. Suery (Editions du Centre Nationale de la Recherche Scientifique, Paris, France, 1985) pp. 5.1–5.13.
30. P. M. HAZZLEDINE, in "Proceedings of the 4th RISO International Symposium on Metallurgy and Materials Science", edited by J. B. Bilde-Sørensen, N. Hansen, A. Horsewell, T. Leffers and H. Lilholt (Risø National Lab., Roskilde, Denmark, 1983) p. 27.
31. J. F. W. BISHOP, *J. Mech. Phys. Solids* **3** (1954) 130.
32. K. MATSUKI, H. MORITA, M. YAMADA and Y. MURAKAMI, *Metal Sci.* **11** (1977) 156.
33. R. C. GIFKINS, in "Superplastic Forming of Structural Alloys", edited by N. E. Paton and C. H. Hamilton (Metals Society AIME, Warrendale, PA, 1982) p. 3.

Received 31 August 1990
and accepted 24 January 1991